Uzbekistan Journal of Polymers

journal homepage: https://uzpolymerjournal.com/
ISSN (online): 2181-3256 (print) 2181-3246

SOL-GEL SYNTHESIS OF CELLULOSE-SILICA COMPOSITES BASED ON MICRO - AND NANOCRYSTALLINE CELLULOSE

Ergashev D.J*., Jumaev A.H**., Atakhanov A.A*., Zhu X***.

**Institute of Polymer Chemistry and Physics Uzbekistan Academy of Sciences, 100128, Tashkent, Uzbekistan[2]*
***University Bayreuth, Germany, Bayern, Universitätsstraße 30, 95447*
*** School of Textile Science and Engineering, Zhejiang Sci-Tech University, China, Zhejiang, Hangzhou, 928 Second Avenue, Xiasha Higher Education Park, 310018*

ARTICLE INFO

Received: 04 March 2025
Revised: 01 July 2025
Accepted: 04 July 2025

Keywords:
Cellulose nanocrystals, microcrystalline cellulose, cellulose-silica composite, hybrid sol-gel material

Corresponding author: Ergashev D.
polymer@academy.uz

ABSTRACT

Sol–gel derived hybrid organic–inorganic materials offer significant advantages for optical and structural applications due to their facile synthesis, ease of shaping and patterning, and excellent mechanical and optical properties. This study focuses on synthesizing novel cellulose-silica composites (CSCs) based on microcrystalline cellulose (MCC), cellulose nanocrystals (CNC), and tetraethoxysilane (TEOS) via a modified sol-gel method. The cellulose suspension was initially prepared by homogenizing MCC and CNC in ethanol, followed by incorporation of hydrolyzed TEOS. The structural and morphological characteristics of the composites were analyzed using atomic force microscopy (AFM), dynamic light scattering (DLS), X-ray diffraction (XRD), thermogravimetric analysis (TGA), and Fourier-transform infrared spectroscopy (FTIR). The results confirm successful integration of cellulose and silica, as well as enhanced thermal stability and modified morphology of the composites.

Introduction

Organic–inorganic composites represent a novel class of hybrid materials that exhibit unique and enhanced properties. The incorporation of an inorganic component into an organic polymer matrix significantly improves the overall characteristics of the polymer. This rapidly evolving field has led to the development of numerous innovative materials with properties that are not merely the sum of their individual constituents, but are also greatly influenced by the nature of the interfacial interactions between phases [1-4]. Organic–inorganic hybrid materials are not only of scientific interest but also offer great potential for industrial applications due to their improved or unconventional properties [5–6]. Among the various materials suitable for hybrid synthesis, cellulose derivatives and silica stand out as particularly effective precursors for sol-gel derived composites. Cellulose — regarded as the most abundant and renewable natural polymer — along with its modified forms such as microcrystalline cellulose (MCC) and cellulose nanocrystals (CNC), has attracted significant attention [7–10]. As the particle size of cellulose decreases through chemical, physical, or mechanical treatments, notable changes occur in its physicochemical and functional properties. These transformations expand its applicability and enable the development of novel materials with tailored characteristics [11–16]. Recent research has increasingly focused on cellulose-based composites, leveraging its intrinsic properties: wide availability, biodegradability, hydrophilicity, and favorable mechanical strength. However, regenerated

cellulose fibers are limited in high-performance applications due to their susceptibility to thermal degradation, ignition, and flammability [17,18].

Silica, on the other hand, has been extensively studied for its versatility and application across various domains, including glass, ceramics, construction materials, rubber fillers, optical fibers, sensors, and chromatographic supports [19,20]. There are three primary approaches to the synthesis of cellulose-silica composites: the sol-gel method, layer-by-layer assembly, and biomineralization-inspired techniques [21]. Among these, the sol-gel process is the most commonly employed technique for fabricating silica-based hybrids, typically using silicon alkoxides as precursors [22], since it combines the control over composition and microstructure at the molecular level with the ability to shape materials under mild and low-energy conditions. Tetraethoxysilane (TEOS), a widely used alkoxide, undergoes hydrolysis to form reactive silanol groups. Subsequent condensation reactions with this group initiate the sol-gel transition, forming a solid silica network (gel). The surface of silica produced via this method contains chemically active silanol groups, enabling their further functionalization with various molecules [23].

The aim of this research is to synthesize cellulose–silica composites via the sol-gel method and investigate their morphology and thermal properties.

Materials and methods

Cellulose nanocrystals (CNC), microcrystalline cellulose (MCC), and tetraethoxysilane (TEOS, $(C_2H_5O)_4Si$) were used as raw materials for the synthesis of cellulose–silica composites (CSCs).

The CNC sample, with a degree of polymerization ranging from 120 to 240, was prepared via hydrolysis of cotton cellulose in a 61% aqueous H_2SO_4 solution at 40 °C, with a cellulose-to-acid ratio (modulus) of 1:10; the reaction was maintained for 90 minutes [24].

MCC, with a degree of polymerization between 240 and 310, was obtained by hydrolyzing cotton cellulose in a 4% aqueous HNO_3 solution at a temperature of 100–110 °C, using a similar 1:10 modulus. The reaction duration was 60 minutes [25].

For preparation of the cellulose suspension, 1.05 g of either CNC or MCC was dispersed in 10 mL of ethanol and homogenized using an IKA Ultra-Turrax Tube Disperser at a rotational speed of 5000 rpm for 1 hour. Simultaneously, TEOS was hydrolyzed by mixing 4 mL of TEOS, 2 mL of 95% ethanol, and 1 mL of 0.1 N HCl. The mixture was stirred at room temperature at 500 rpm for 1 hour to generate reactive silanol groups.

To synthesize the cellulose–silica composite, the prepared cellulose suspension was added to the TEOS solution under continuous stirring. After 10 minutes of mixing, 0.1 mL of a 1 N NH_4OH solution was introduced to initiate gelation. The resulting mixture was washed several times with distilled water and ethanol, and dried at 100–105 °C (Scheme 1)

FTIR studies were carried out on an Inventio-S IR Fure spectrometer (Bruker, Germany) in the wavelength range from 500 cm^{-1} to 4000 cm^{-1}.

XRD studies were carried out using an XRD Miniflex 600 (Rigaku, Japan) with monochromatic CuKα radiation isolated by a nickel filter with a wavelength of 1.5418 Å at 40 kV and the current strength of 15 mA. The spectrum was recorded in the interval $2\theta = 5^{\circ}–40^{\circ}$. The data processing of experimental diffraction patterns, peak deconvolution, describing the peaks used by Miller indices, peak shape, and the basis for the amorphous contribution were conducted using the software “SmartLab Studio II” and data base PDF-2 (2020 Powder diffraction file, ICDD).

Thermal analysis and derivative thermogravimetry analysis of the composite was carried out on a universal thermo analytical device STA TG-DTA/DSC “Start-1600” (Linseis, Germany) at a heating rate of 10 °C min^{-1} in flowing air. Temperature scanning of the samples was carried out in an air atmosphere in the temperature range of 20-800°C.

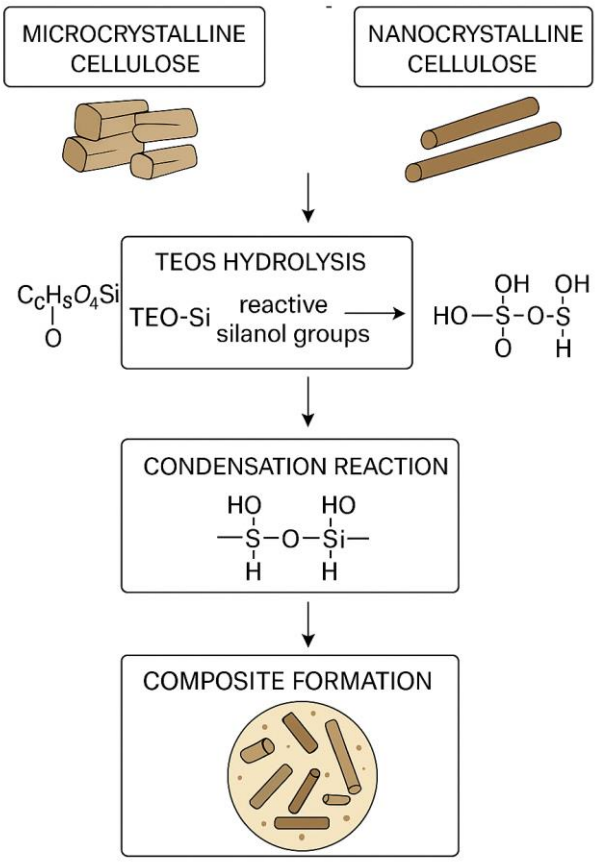

Scheme 1. Synthesis of the cellulose–silica composite

Particle size distribution was measured using a Photocor Compact system (Photocor, Russia) equipped with a thermally stabilized 25 mW laser (λ = 635.6 nm) at 298 K.

The morphology of the samples was studied using an Agilent 5500 atomic force microscope (Agilent, USA). A silicon cantilever with a force of 9.5 N/m2 and a frequency of 145 kHz was used in the research work. A 25-25-1 μm area was scanned in the ACM along the x-y-z coordinates.

Results and discussion

The FTIR spectra of MCC and CNC samples (Fig. 3) exhibit characteristic valence and deformation vibrations typical of cellulose. These include absorption bands corresponding to C–H stretching in methylene and methine groups around 2903 cm^{-1}.

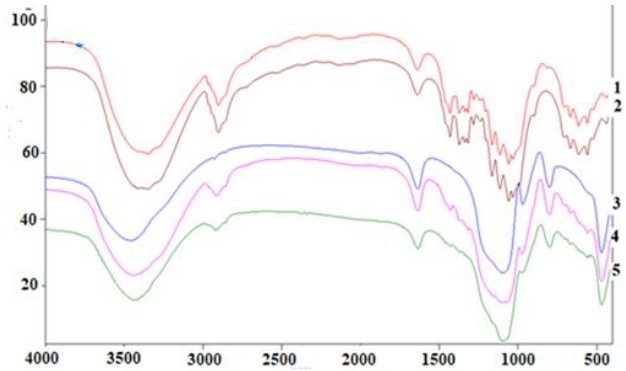

Figure.1. FTIR spectra of MCC, CNC, SiO_2 and CSC samples.
1. MCC; 2. CNC; 3. SiO_2; 4. MCC - SiO_2; 5. CNC -SiO_2;

In the FTIR spectrum of pure SiO_2, distinct valence and deformation vibrations were observed, differing from those of cellulose. Notably, strong peaks were identified at approximately 790 cm^{-1} and 1100 cm^{-1}, which correspond to Si–O–Si stretching vibrations, confirming the presence of silica.

In the spectra of the cellulose–silica composites, bands associated with both cellulose and SiO_2 were detected. The presence of C–H stretching vibrations around 2903 cm^{-1}, alongside the Si–O–Si peaks at 790 cm^{-1} and 1100 cm^{-1}, suggests successful chemical bonding between the organic and inorganic phases. Additionally, a peak at approximately 470 cm^{-1}, also associated with Si–O–Si bending, further supports the integration of silica into the cellulose matrix [26–28]. Furthermore, in the FTIR spectra of the composites, the intensity of the broad –OH stretching band around 3442 cm^{-1} decreased, indicating reduced availability of free hydroxyl groups. This is likely due to hydrogen bonding or condensation reactions with silanol groups. A reduction in the intensity of the peak at 1635 cm^{-1}, which is typically associated with adsorbed water, was also observed, indicating a lower moisture content in the composite materials.

To further investigate and compare the amorphous and crystalline structures of the cellulose–silica composites, X-ray diffraction (XRD) analysis was performed (Fig. 2).

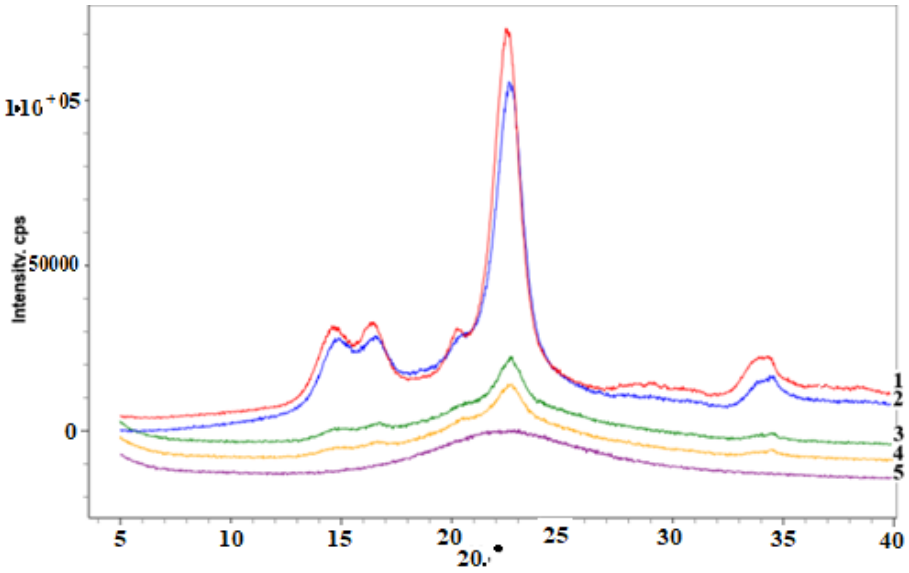

Figure 2. Diffraction patterns of MCC, CNC, SiO_2 and CSC.
1. CNC; 2. MCC; 3. CNC-SiO_2; 4. MCC-SiO_2; 5. SiO_2;

X-ray diffraction (XRD) analysis confirmed that both microcrystalline cellulose (MCC) and cellulose nanocrystals (CNC) exhibited characteristic crystalline peaks associated with the native cellulose I structure. These sharp and well-defined reflections indicate a high degree of crystallinity in both materials.

In contrast, the XRD pattern of silica (SiO_2) synthesized via the sol–gel method using TEOS displayed a broad, diffuse halo in the 2θ range of 5° to 40°, which is indicative of an amorphous structure. This result confirms that the synthesized silica lacks long-range crystalline order, as is typical for sol–gel derived silica.

For the cellulose–silica composites (CSCs), the incorporation of SiO_2 into the cellulose matrix resulted in a noticeable reduction in crystallinity. Specifically, the crystallinity index of the MCC-based composite decreased from 71% (neat MCC) to 18%, while the CNC-based composite showed a reduction from 86% (neat CNC) to 20%. This significant decline suggests that the silica matrix interferes with the regular packing of cellulose chains, partially disrupting the crystalline regions.

Additionally, a slight shift in the main cellulose diffraction peak was observed, moving from $2\theta = 22.58°$ in pure cellulose to $2\theta = 22.63°$ in the composites. This shift may indicate slight changes

in the interplanar spacing, possibly due to the formation of hydrogen bonds or covalent interactions between cellulose hydroxyl groups and the silanol moieties of the silica network.

These findings support the hypothesis that the sol–gel process leads to a successful embedding of amorphous silica within the cellulose matrix, altering the structural order and decreasing the degree of crystallinity

Figure 3 presents the thermogravimetric analysis (TGA) and differential scanning calorimetry (DSC) results for the CNC, MCC, and their corresponding cellulose–silica composites, further illustrating changes in thermal behavior due to hybridization

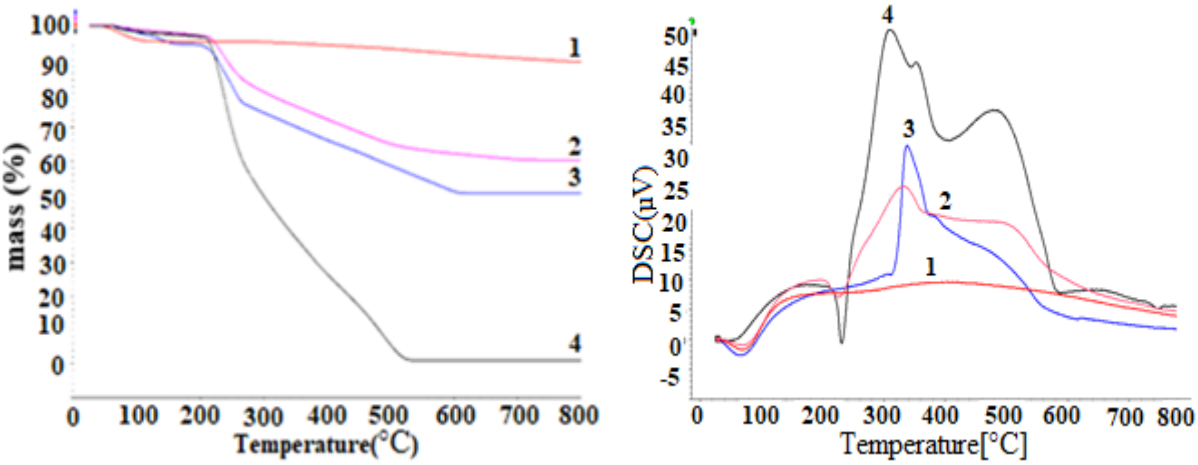

Figure 3. TG and DSC curves of CNC, SiO_2 and CSC samples.
1. SiO_2; 2. CNC -SiO_2; 3. MCC-SiO_2; 4. CNC

Thermal analysis of the cellulose–silica composites revealed three distinct stages of weight loss, as shown in the thermogravimetric (TG) and differential scanning calorimetry (DSC) curves [29]. These stages correspond to (1) moisture desorption, (2) thermal degradation of the organic matrix, and (3) complete decomposition of cellulose.

The initial weight loss, occurring between 60–150 °C, is attributed to the release of physically adsorbed water. This stage is common in cellulose-based materials due to their hydrophilic nature.

The second stage, which reflects the primary thermal degradation of cellulose, varies depending on the material composition. For pure MCC, degradation occurs between 295–315 °C. In MCC–silica composites, this range shifts slightly higher to 305–345 °C, indicating enhanced thermal resistance. For CNC–silica composites, degradation occurs at an even higher range of 325–375 °C. The delayed onset of decomposition in the composites demonstrates a significant improvement in thermal stability, which can be attributed to strong interactions — likely hydrogen bonding or partial covalent linking — between cellulose and the silica network.

Notably, no thermal degradation was observed for pure SiO_2 in the studied temperature range, consistent with its known high thermal stability. The increased decomposition temperatures in the composites further confirm the effective integration of silica into the cellulose matrix and the formation of thermally stable organo–inorganic hybrid structures.

A small endothermic peak around 94 °C was observed in all samples, corresponding to water evaporation. In the composites, endothermic transitions between 310–340 °C likely reflect structural rearrangements or segmental motion of the cellulose chains during decomposition. A broad exothermic peak spanning 340–700 °C was also noted, correlating with significant mass loss in the TG curves and associated with the final decomposition of the carbonaceous residue.

We focused on synthesizing silica composites based on CNC and MCC using different amounts of silica precursor. For this purpose, we prepared a series of composite samples by varying the molar ratios between cellulose (CNC or MCC) and the silica precursor (TEOS) as 1:1.2, 1:1.4,

1:1.6, 1:1.8, and 1:2. This approach allowed us to systematically explore the effect of cellulose-to-silica ratio on the structural and thermal properties of the resulting composites.

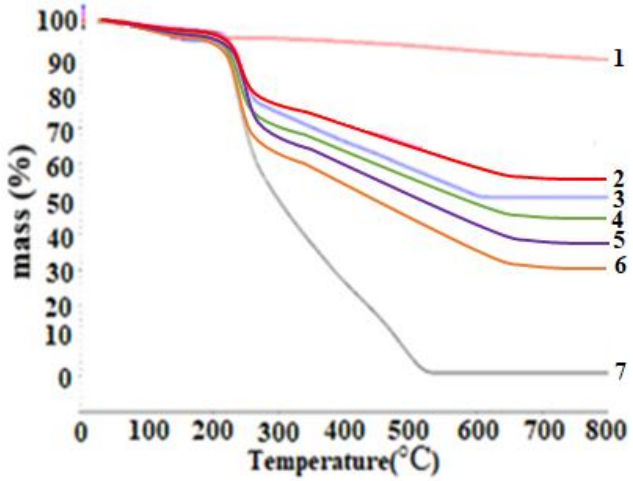

Figure 4. TG curves of the composites obtained based on the molar ratios between CNC and TEOS. 1). SiO_2; 2). 1:2; 3). 1:1.8; 4). 1:1.6; 5). 1:1,4; 6). 1:1.2; 7). CNC

Our thermogravimetric analysis (TGA) data clearly demonstrated that increasing the silica content within the cellulose matrix led to enhanced thermal stability of the composites. The decomposition temperature shifted progressively to higher values with increasing silica loading, indicating improved thermal resistance due to the formation of an increasingly interconnected silica network surrounding the cellulose structure. Thermal stability enhancement with increasing TEOS content is in agreement with previous studies on similar hybrid systems, where the inorganic silica phase acts as a thermal barrier and inhibits the mobility and degradation of cellulose chains. Representative thermogravimetric curves of the composite samples are presented below to illustrate this trend.

The overall thermal behavior suggests that the incorporation of silica into cellulose matrices not only enhances thermal resistance but also broadens the thermal operating window of the composites. These findings highlight the potential of cellulose–silica hybrids for use in high-temperature applications, including flame-retardant coatings, thermal insulation materials, and composite engineering components [30,31].

Dynamic light scattering (DLS) analysis was performed to determine the hydrodynamic diameter and translational diffusion coefficients of particles in the dispersed phase. The measurements were used to assess particle size distribution in the neat components (CNC and SiO_2) and the resulting CSC. The data are summarized in Table 1.

Table 1

Particle size distribution

Samples	Quantity, %	R, nm	Diffusion coefficient, Dt(cm^2/s)
NC	70	156	$1.773x10^{-12}$
SiO_2	65	178	$1.556\ x10^{-12}$
CSC	56	206	$1.351\ x10^{-12}$

The DLS measurements revealed that the particle sizes of all samples ranged from the lower nanometer scale toward submicron dimensions, with notable differences among the components. The CNC exhibited a relatively narrow distribution centered at 156 nm. In contrast, SiO_2 particles synthesized via the sol–gel method showed a slightly larger average size of 178 nm, reflecting the inherent nature of the hydrolyzed and condensed TEOS-derived silica network.

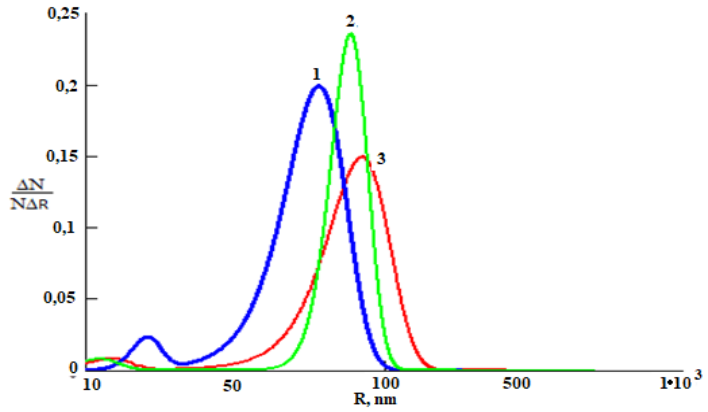

Figure 5. Results of the analysis of dynamic light scattering of CNC, SiO_2 and CNC-SiO2 samples. 1. CNC 2. SiO_2 3. CNC - SiO_2

Upon formation of the composite (CSC), the average particle size further increased to 206 nm, accompanied by a decrease in the diffusion coefficient. This increase in hydrodynamic radius is indicative of successful integration and encapsulation of cellulose structures by the silica matrix. It also suggests possible agglomeration or surface modifications caused by the hybridization process.

The fluctuations in scattering intensity as a function of time confirmed a consistent diffusion behavior, and the resulting size distributions suggested that the system maintained colloidal stability during measurement. The broader size range observed in the composites, relative to the neat CNC or SiO_2, reflects a more heterogeneous distribution, which is typical for sol–gel derived hybrid materials.

These results reinforce the conclusion that cellulose and silica interact effectively during the sol–gel process, yielding stable hybrid nanoparticles with increased particle size and slightly reduced diffusion mobility due to their more complex morphology and increased molecular weight.

Atomic force microscopy (AFM) was employed to investigate the surface morphology and nanoscale structure of the CNC and their silica-modified composites (CNC–SiO_2). The results reveal significant morphological changes upon composite formation.

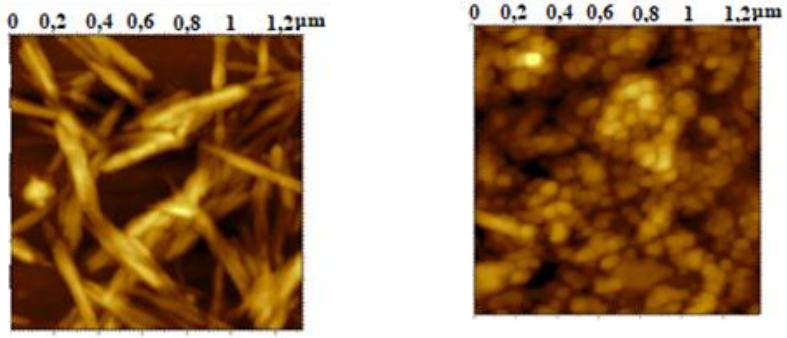

Figure 6. AFM images of CNC and CNC-SiO_2 samples.

The unmodified CNC sample exhibited a typical rod-like morphology, consistent with literature reports on nanocrystalline cellulose derived from acid hydrolysis. These elongated particles had relatively uniform dimensions and were well-dispersed across the scanned surface, reflecting their nanoscale size and colloidal stability.

In contrast, the morphology of the cellulose–silica composite (CNC–SiO_2) changed dramatically. The AFM images showed a transition from rod-like to predominantly spherical structures. This transformation is attributed to the deposition and condensation of silica around the

cellulose nanocrystals during the sol–gel process. The resulting spherical features are indicative of encapsulation or surface coating of CNCs by the silica phase.

The particle dimensions remained within the nanometer scale, further validating the successful formation of nanosized hybrid structures. This morphological evolution suggests strong interfacial interactions between cellulose and silica, which may include hydrogen bonding or partial covalent linkage via silanol groups.

The observed spherical shape in the composites may also contribute to improved thermal and mechanical properties, as more isotropic particle geometries can enhance packing density and stress distribution in potential composite matrices.

These findings support the conclusions from the FTIR, XRD, and DLS analyses and demonstrate the structural integration of silica into the cellulose framework at the nanoscale level.

In order to evaluate the pore structure and specific surface area of the synthesized MCC–SiO_2 and CNC–SiO_2 composites, an isothermal analysis based on benzene adsorption was performed. This analysis was carried out by recording adsorption–desorption isotherms in the gas phase, and the results were calculated using the BET (Brunauer–Emmett–Teller) and BJH (Barrett–Joyner–Halenda) models. During the process, benzene vapor was adsorbed at various relative pressures, allowing the determination of monolayer capacity (Am), specific surface area (S), micropore and mesopore volumes (Wmic, Wmezo), saturation volume (Vs), and average pore radius (rk). The table below presents the comparative values of these parameters for the neat and composite samples based on MCC and CNC.

Table 2

Isothermal analysis results of the composite samples based on benzene adsorption

№	Indicators	MCC	MCC-SiO_2	CNC	CNC-SiO_2
1	Am (monolayer capacity), mmol/g	0.256	1.204	0.066	0.541
2	Specific surface area S, m^2/g	61.76	321.3	15.06	128.2
3	Micropore volume W(mic), cm^3/g	0.057	0.248	0.015	0.102
4	Saturation volume Vs	0.078	0.414	0.023	0.132
5	Mesopore volume Wmezo, cm^3/g	0.02	0,11	0.01	0,05
6	Pore radius rk, Å	25.3	20.4	31.3	20.8

The results of the isothermal analysis based on benzene adsorption presented in Table 1 indicate that the silica-modified composites (MCC–SiO_2 and CNC–SiO_2) exhibit a significantly increased sorption capacity compared to their unmodified counterparts (MCC and CNC). The monolayer capacity (Am) for the MCC sample was 0.256 mmol/g, which increased to 1.204 mmol/g in the MCC–SiO_2 composite. Similarly, for the NC sample, Am was 0.066 mmol/g, while in the CNC–SiO_2 composite, it rose to 0.541 mmol/g. This enhancement suggests that the addition of silica increases the number of active surface sites, thereby significantly improving the sorption capacity. An increase in the specific surface area (S) was also observed: from 61.76 m^2/g in MCC to 321.3 m^2/g in the MCC–SiO_2 composite, and from 15.06 m^2/g in NC to 128.2 m^2/g in the CNC–SiO_2 composite. This expansion of the surface area contributes directly to improved adsorption performance. The micropore volume (Wmic) also increased considerably upon silica modification, indicating the development of a more extensive microporous network. Furthermore, the reduction in pore radius — from 25.3 Å in MCC to 20.4 Å in MCC–SiO_2, and from 31.3 Å in NC to 20.8 Å in CNC–SiO_2 — can be attributed to the formation of a greater number of smaller pores. This structural change enhances the surface activity and facilitates more effective adsorption interactions.

Conclusions

Cellulose–silica composites were successfully fabricated via a straightforward sol–gel approach, combining cellulose (microcrystalline and nanocrystalline) with tetraethoxysilane. Structural analyses (FTIR, XRD) confirmed the incorporation of amorphous silica into the cellulose matrix, resulting in a marked reduction in cellulose crystallinity and evidence of strong interfacial bonding. Morphological studies (DLS, AFM) demonstrated that hybridization increased particle size and transformed the native rod-like cellulose nanocrystals into more isotropic, spherical composites. Thermal characterization (TGA/DSC) revealed substantially enhanced thermal stability for the composites compared to pure cellulose, with degradation onset temperatures shifted to higher values.

Collectively, these findings illustrate that the sol–gel route produces well-integrated cellulose–silica hybrids with tailored structural and functional properties. The pronounced improvements in thermal stability, coupled with controlled nanoscale morphology and tunable crystallinity, position these composites as promising candidates for high-temperature applications, advanced coatings, optical materials, and other fields requiring durable, hybrid organic–inorganic systems.

The results of the isothermal analysis based on benzene adsorption indicate that the sorption properties of MCC–SiO_2 and CNC–SiO_2 composites have significantly improved due to the incorporation of silica. Increases in parameters such as monolayer capacity (Am), specific surface area (S), and micropore volume (Wmic) confirm the rise in the number of active sites and the development of a more extensive surface. Additionally, the decrease in pore radius suggests the formation of smaller pores, which enhances the overall adsorption efficiency of the materials. These changes demonstrate the successful integration of the silica component into the cellulose matrix.

REFERENCES

[1]. Innocenzi P., Lebeau B. // Organic–inorganic hybrid materials for nonlinear optics. J Mater Chem., 2005, № 15, pp 3821–31, doi.org/10.1039/B506028A

[2]. Bauer F., Decker U., Ernst H., Findeisen M., Langguth H., Mehnert R. // Functionalized inorganic/organic nanocomposites as new basic raw materials for adhesives and sealants . 2006, № 26, pp. 567–70, doi.org/10.1016/j.ijadhadh.2005.11.001

[3]. Elsevier B.V. // Hybrid Polymer–Inorganic Nanostructures. U Wiesner, Cornell University, Ithaca, NY, USA., 2012, № 65, pp. 491–516, doi.org/10.1016/B978-0-444-53349-4.00179

[4]. Sanchez C., Julı´an B., Belleville P., Popall M. // Applications of hybrid organic–inorganic nanocomposites. J Mater Chem., 2005, № 15, pp. 3559–92, DOI:10.1039/B509097K

[5]. H. S. Barud, R. M. N. Assunc, M. A. U. Martines, J. Dexpert-Ghys, R. F. C. Marques, Y. Messaddeq, S. J. L. Ribeiro. // Bacterial cellulose–silica organic–inorganic hybrids. Sol-Gel SciTechnol., 2008, № 46, pp. 363–367, DOI:10.1007/s10971-007-1669-9

[6]. Sónia S., Dmitry V., Evtuguin, Inês P., Ana Esculcas P. // Synthesis and characterisation of cellulose/silica hybrids obtained by heteropoly acid catalysed sol–gel process. Materials Science and Engineering., 2007, V 27, № 1, pp. 172-179, doi.org/10.1016/j.msec.2006.04.007

[7]. Hussain A., Calabria-Holleya J., Schorr D., Jianga Y., Lawrence and Blanchet P. // Hydrophobicity of hemp shiv treated with sol-gel coatings. Applied Surface Science., 2018, № 434, pp. 850-860, DOI:10.1016/j.apsusc.2017.10.210

[8]. Wen X.F., Wang K., Pi P.-H., Yang J.-X., Cai Z.-Q., Zhang L.-J., Qian Y., Yang Z.-R., Zheng D.-F., Cheng J. // Organic-inorganic hybrid superhydrophobic surfaces using methyltriethoxysilane and tetraethoxysilane sol-gel derived materials in emulsion. Appl. Surf. Sci., 2011, № 55, pp. 991–998, doi.org/10.3390/coatings9100627

[9]. Dieter K., Brigitte H., Hans-Peter F., Andreas B. // Cellulose: fascinating biopolymer and sustainable raw material. Affiliations expandPMID., 2005, № 30, Pp. 3358-73, DOI: 10.1002/anie.200460587

[10]. Ayu G.E., Nasution H., Lubis M., Harahap H and Al Fath M.T. // The Production of Nanocrystalline Cellulose From Oil Palm Fruit Fibers Using Chemical Treatment. AIP Conference Proceedings., 2020, № 22, 67 020036, https://doi.org/10.1063/5.0015667

[11]. Atakhanov A. A., Kholmuminov A. A., Mamadiyorov B. N., Turdikulov I. Kh., and Ashurov N. Sh. // Rheological Behavior of Nanocellulose Aqueous Suspensions. POLYMER SCIENCE. SERIES C, 2020, Vol 62, № 3, pp. 189-195, https://DOI: 10.1134/S0965545X20030013

[12]. Hasani M., Cranston E.D., Westman G., Gray D.G. // Cationic Surface Functionalisation of Cellulose Nanocrystals. Soft Matter., 2008, №4, pp. 2238–2244, DOI: 10.1039/b806789a.
[13]. Атаханов А.А., Мамадиёров Б., Кузиева М., Югай С.М., Шахобутдинов С., Ашуров Н.Ш., Абдуразаков М. // Сравнительные исследования физико-химических свойств и структуры хлопковой целлюлозы и ее модифицированных форм. Химия растительного сырья., 2019, №3, С. 5–13, doi: 10.14258/jcprm.2019034554
[14]. Мамадиёров Б.Н., Эргашев Д.Ж., Саидмухаммедова М.Қ., Ашуров Н.Ш., Атаханов А.А. // Сомон целлюлозасидан микро- ва нанокристаллик целлюлоза олиш ва хоссаларини тадқиқ қилиш. «Илм-фан ва инновацион ривожланиш» илмий журнали., 2022, № 4, С. 5-17, doi:https://dx.doi.org/10.36522/2181-9637-2022-4-1.
[15]. Morais J.P.S., Rosa M.F., Filho M.M.S., Nascimento L.D., Nascimento D.M., Cassales A.R. // Extraction and characterization of nanocellulose structures from raw cotton linter. Carbohydrate Polymers., 2013, №91, pp. 229–235, DOI:10.1016/j.carbpol.2012.08.010.
[16]. Аутлов С.А., Базарнова Н.Г., Кушнир Е.Ю. // Микрокристаллическая целлюлоза: структура, свойства и области применения (обзор). Химия растительного сырья., 2013, №3, pp. 33–41, DOI: 10.14258/jcprm.1303033.
[17]. Сарымсаков А. А., [и др.]. // Диспергированная микрокристаллическая целлюлоза и гидрогели на ее основе. Химия растительного сырья., 2014, № 2, pp. 11–16,
[18]. Атаханов А. А. // Получение, структура, свойства и технология производства хлопковой, микрокристаллической и наноцеллюлозы. автореф. дис. д-ра техн. наук: 02.00.12. Ташкент, 2016, 31 с.
[19]. Pinto, R. J. B., Marques, P. A. A. P., Barros-Timmons, A. M., Trindade, T., and Neto, C. P. // Novel SiO2/cellulose nanocomposites obtained by in situsynthesis and via polyelectrolytes assembly. Comp. Sci. Technol., 2008, № 68, pp. 1088-1093, DOI:10.1016/j.compscitech.2007.03.001
[20]. Hribernik, S., Smole, M. S., Kleinschek, K. S., Bele, M., Jamnik, J., and Gaberscek, M. // Flame retardant activity of SiO2-coated regenerated cellulose fibres. Polym. Degrad. Stabil., 2007, № 92, pp. 1957-1965, DOI:10.1016/j.polymdegradstab.2007.08.010
[21]. Rosaria C., Alexandra F., Valerica P., Franç ois B. L., Laura M. I., Mario P. // The Sol−Gel Route to Advanced Silica-Based Materials and Recent Applications. Chem. Rev., 2013, № 113, pp. 6592−6620, doi: 10.1021/cr300399c.
[22]. Hussain A., Calabria-Holleya J., Schorr D., Jianga Y., Lawrence and Blanchet P. // Hydrophobicity of hemp shiv treated with sol-gel coatings. Applied Surface Science. Applied Surface Science., 2018, № 434, pp. 850-860, https://doi.org/10.1016/j.apsusc.2017.10.210
[23]. Vasquez A., Cyras V. P., Alvarez V. A., and Moran J. I. // Starch/clay nano-biocomposites," in Environmental Silicate Nano-Biocomposites. L.Av´ erous and E. Pollet, Eds., chapter 11.14, Springer, London, UK, 1st edition., 2012, pp. 287–321, https://doi.org/10.1155/2015/493439
[24]. Atakhanov A, Turdikulov I, Mamadiyorov B, Abdullaeva N, Nurgaliev I, Khaydar Y, Rashidova S, Isolation of Nanocellulose from Cotton Cellulose and Computer Modeling of Its Structure. Open Journal of Polymer Chemistry. 2019, 9:117-129. doi: 10.4236/ojpchem.2019.94010.
[25]. Ataxanov A.A. "Paxta-Mikrokristallik, va Nanosellyulozaning olinishi, tuzilishi, xossalari va ishlab chiqarish texnologiyasi" doctoral thesis abstract, 2016, 50 b.
[26]. Kyung-Soo K., Jun-Kyung K., Woo-Sik K. // // Influence of reaction conditions on sol-precipitation process producing silicon oxide particles. Ceramics International., 2002, V 28, № 2, pp. 187-194, https://doi.org/10.1016/S0272-8842(01)00076-1
[27]. Masoud M., Malihe B. Z., Mahdieh D., Khalilollah S., Seyed T. K., Jalil S. , Azadeh F., and Hajar M. // Silica Mesoporous Structures: Effective Nanocarriers in Drug Delivery and Nanocatalysts. Applied sciences., 2020, №10, 7533, doi:10.3390/app10217533
[28]. Joabel R., Alessandra S.F., Lina B., Caue R., Maria A. M., José M.M., Gustavo H., Denzin T. // Evaluation of reaction factors for deposition of silica (SiO2) nanoparticles on cellulose fibers. Carbohydrate Polymers., 2014, T 114, № 1, pp. 424–431, https://doi.org/10.1016/j.carbpol.2014.08.042.
[29]. Musawenkosi G.Sh., Nduduzo L.Kh., Samson M.M and Tshwafo E.M. // Factors Affecting Silica/Cellulose Nanocomposite Prepared via the Sol–Gel Technique: A Review. 2024, *17*(9), 1937 https://doi.org/10.3390/ma17091937
[30]. Shi J.Lu.L., Guo W., Zhang J., Cao Y. // Heat insulation performance, mechanics and hydrophobic
[31]. modification of cellulose–SiO2 composite aerogels.Carbohydrate Polymers., 2013. № 98. Pp 282–289. DOI: 10.1016/j.carbpol.2013.05.082
[32]. Ning Jia., Shu-Ming Li., Ming-Guo Ma., Jie-Fang Zhu., and Run-Cang Suna. " Synthesis, cellulose silica composite,"bioresources 2011. 6(2), 1186-1195. DOI:10.15376/biores.6.2.1186-1195